Nuclear Magnetic Resonances and Mn-O-P-O-Mn Superexchange Linkages in Paramagnetic and Antiferromagnetic $LiMnPO_4$

JOHN M. MAYS*
Bell Telephone Laboratories, Murray Hill, New Jersey
(Received 28 February 1963)

Nuclear magnetic resonances of P^{31} and Li^7 have been observed in single crystals of $LiMnPO_4$ in the antiferromagnetic and paramagnetic states as a function of orientation from 4.2–300°K. The resonances were found to be shifted from the predicted γH_0 in a way that indicates the presence of unpaired electrons in $3s$ (and possibly $3p$) orbitals of the phosphorus atoms separated from the magnetic Mn^{++} ions by an intervening oxygen atom. The Néel temperature is established as 34.85°±0.1°K by observation of the Li^7 resonance as a function of temperature. The arrangement of spins in the antiferromagnetic state is established by a combination of NMR and susceptibility data. The structure so determined requires the presence of superexchange interactions along Mn-O-P-O-Mn paths as well as conventional Mn-O-Mn paths. Discussion is given of the observed shifts in terms of chemical bonding and of the connection between the shifts and both the conventional and longer range superexchange linkages. Linewidths and shapes and values of T_1 are given and discussed briefly.

1. INTRODUCTION

IN paramagnetic crystals the local magnetic field at the nucleus of a nonmagnetic ion is in general different from the applied field $\mathbf{H}_0$. This difference arises from the presence of unpaired electronic spins. If the unpaired electrons are localized on the magnetic ions the field at the nuclear site, the so-called dipole sum, is calculable in a single crystal from susceptibilities and the crystal structure. If the unpaired electrons have spread out by some mechanism onto the nonmagnetic ions, the effective field at the nucleus of these ions will be changed by an amount that depends upon the quantity and state of unpaired electrons present on the ion and on the hyperfine interaction of the electrons with the nucleus. The shift of the nuclear magnetic resonance (NMR) frequency from its normal value $\omega=\gamma H_0$ is a measure of these internal fields. The proton resonance in $CuSO_4\cdot 5H_2O$ and $CuCl_2\cdot 2H_2O$ are examples of cases where the experimental data can be explained without the necessity of assuming the presence of any unpaired electrons on the protons.[1] Shulman and Jaccarino[2] subsequently observed the fluorine NMR in MnF_2 and showed that the rather large shifts could be explained only by assuming the presence of unpaired $2s$ and $2p$ electrons on the fluorine atom. They showed also that the presence of such unpaired electrons on nonmagnetic ions in an antiferromagnetic salt fitted in well with the idea that the superexchange forces producing antiferromagnetism involve interaction of unpaired electrons on intervening nonmagnetic ions.[3,4]

Subsequently, the present author observed similar large shifts in the phosphorus NMR in a number of synthetic powder and mineral samples of iron group phosphates.[5] These observations showed that unpaired electrons were making themselves felt at sites separated by another nonmagnetic ion (oxygen) from the magnetic ion. The temperature dependence of the shifts in the mineral of known structure[6,7] lithiophilite Li(Mn,Fe)PO_4 from room temperature to 77°K suggested that this compound undergoes an antiferromagnetic transition below 77°K. The existence of such a transition was established by susceptibility measurements by Bozorth and Kramer.[8] The present investigation of nuclear resonances in a single crystal of $LiMnPO_4$ was undertaken to study in detail these large NMR shifts at second nearest neighbor sites and their connection, if any, with the superexchange forces producing the observed antiferromagnetism.

$LiMnPO_4$ has the orthorhombic olivine structure.[7] There are four formula weights per unit cell. The four Mn^{++} ions are crystallographically equivalent as are the four Li^+ ions and the four phosphorus atoms. The sixteen oxygen atoms are divided in the ratio 4-4-8 among three sets of crystallographically equivalent sites. Manganese ions are surrounded by distorted octahedra of oxygen atoms and so also are the lithium ions. Phosphorus is, of course, tetrahedrally surrounded by oxygen atoms to form PO_4^{3-} groups. Typical coordination around Mn, Li, and P is shown in Fig. 1. Each of the lithium ions lies at a center of inversion and the configurations around the four in the unit cell are related by reflections in the xy, xz, and yz planes. Configurations around the four phosphorus atoms in the unit cell are similarly related to one another. Manganese ions lie in puckered planes perpendicular to the x axis (cf., Figs. 1 and 2). Successive planes are separated by PO_4 tetrahedra and LiO_6 octahedra.

---

* Present address: National Science Foundation, Washington, 25, D. C.

[1] E. R. Andrew, *Nuclear Magnetic Resonance* (Cambridge University Press, Cambridge, England, 1955), pp. 185–190.
[2] R. G. Shulman and V. Jaccarino, Phys. Rev. **108**, 1219 (1957).
[3] P. W. Anderson, Phys. Rev. **79**, 350 (1950).
[4] P. W. Anderson, Phys. Rev. **115**, 2 (1959).
[5] J. M. Mays, Phys. Rev. **108**, 1090 (1957).
[6] A. Byström, Arkiv. Kemi, Mineral. Geol. **17**, 1 (1943).
[7] S. Geller and J. L. Durand, Acta Cryst. **13**, 325 (1960).
[8] R. M. Bozorth and V. Kramer, *Colloque international de magnétisme de Grenoble, 1959*, p. 329.

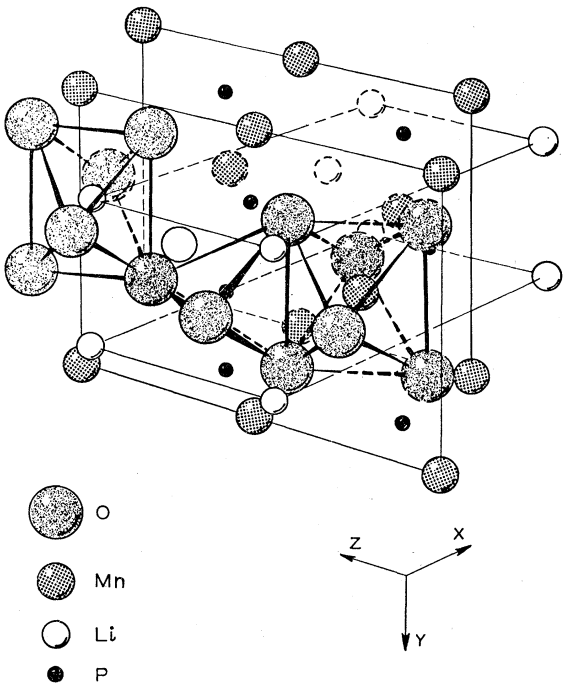

FIG. 1. Typical coordination figures around Mn, Li, and P atoms in $LiMnPO_4$. Unit cell corners are at the eight extreme Li positions.

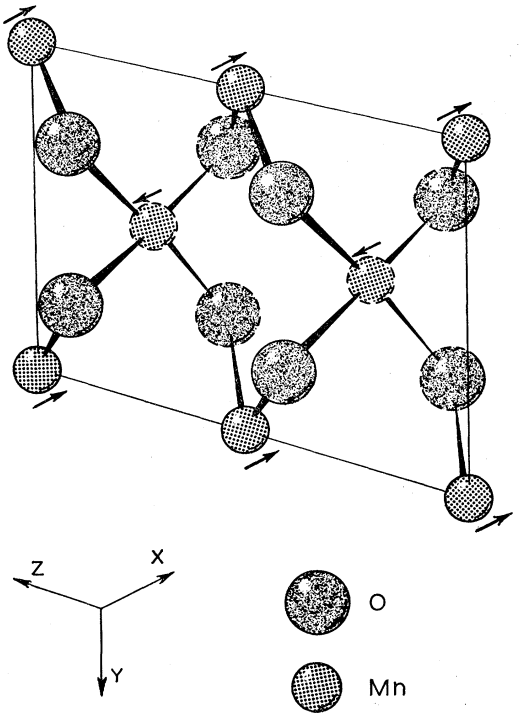

FIG. 2. Puckered plane of Mn atoms and connecting oxygen atoms. Arrows give directions and relative senses of electron spins in antiferromagnetic state.

2. EXPERIMENTAL PROCEDURE

The magnet used was a Varian Associates Model V-4012-3B 12-in. electromagnet with pole caps tapered to 6 in. and a gap of ~2 in. Fields up to 16 kG were obtainable. A Varian Associates variable-frequency induction spectrometer with frequency range 2–16 Mc/sec was used for the measurements.

Single-crystal samples were grown by Dr. J. W. Nielsen of these laboratories by the method of Zambonini and Malossi.[9] Three spherical samples of diameters 0.171, 0.188, and 0.202 in. were prepared by John L. Durand, using the method of Bond.[10] The samples were mounted on sapphire rods with silica cement. The spheres were oriented in such a way as to allow $\mathbf{H}_0$ the external field to be varied in the xy, xz, and yz planes. Measurements were made in a stainless steel Dewar built by the Hofman Laboratories, Newark, New Jersey. The Dewar had a glass tip. The bottom 2 inches were a single Dewar small enough ($\sim\frac{5}{8}$ in.) in diameter to fit easily into the Varian Associates probes. In some of the experiments the tip was unsilvered. In others the inside surface of the outer glass was silvered and then cross-hatched with a scriber to minimize the effect of the silver on the rf. This silvering doubled the working time for a filling of He.

[9] Zambonini and Malossi, Z. Krist. **80**, 442 (1931).
[10] W. L. Bond, Rev. Sci. Instr. **25**, 401 (1954).

3. RESONANCES IN THE PARAMAGNETIC STATE

Theory

In their work on NMR in MnF_2 Shulman and Jaccarino[2] were, as we have said, able to fit the observed data by describing the effective field at the fluorine nucleus in terms of the external field, the field due to the time averaged spins localized on Mn ions, and the hyperfine interaction of unpaired electrons on the fluorine ion. We shall use this picture in discussing the lithium and phosphorus NMR in $LiMnPO_4$. The susceptibility will be taken as isotropic as in MnF_2 (it is pointed out in Appendix A that any anisotropy is very small). If the unpaired spins are taken to be localized at the Mn sites the i component of the effective field at a Li or P site is

$$H^i = H_0{}^i = \sum_j (D^{ij} + \kappa A^{ij}) \langle \mu_j \rangle + \kappa A^s \langle \mu \rangle, \qquad (1)$$

where i, j refer to x, y, z axes. $\langle \mathbf{u} \rangle$ is the time average magnetic moment of the Mn ion and in the paramagnetic state equals $\chi_m \mathbf{H}_0/N$ (see Appendix A). D^{ij} is one of the six components of the symmetric dipole sum tensor; it is shape-dependent and we take the shape to be spherical. To take account of a shift of magnetism from the magnetic ion to other atoms the D^{ij} of (1) must be taken as

$$D^{ij} = \sum_k D_k{}^{ij} f_k, \qquad (2)$$

where f_k is the fraction of the total magnetism assigned to sites of type k and $D_k{}^{ij}$ refers to the dipole sum at the site in question due to magnetism on atoms at sites of type k. A^{ij} is one of the six components of the symmetric tensor describing the anisotropic hyperfine interaction and $\kappa=1/g\beta\gamma\hbar$. A^s refers to the isotropic part of the hyperfine interaction. In the present crystal the following relationships hold for both **D** and **A** tensors in going from one lithium site a in the unit cell to another lithium site b and similarly for phosphorus.

$$D_a{}^{ii}=D_b{}^{ii} \quad |D_a{}^{ij}|=|D_b{}^{ij}|. \tag{3}$$

The contribution of a given atom to D^{ii} is $(3l_i{}^2-1)/r^3$ and to D^{ij} is $3l_il_j/r^3$, where r is the length and l_x, l_y, l_z are the direction cosines of the vector connecting the atom at which the dipolar field is sought to the atom producing the field. These contributions are summed over magnetic ions in the crystal using a Bell Telephone Laboratories program based on the method of Ewald and Shockley.[11] Expressions for the hyperfine interaction are as follows:

$$A^{ii}=\sum(3l_{ik}{}^2-1)A_k \quad A^{ij}=\sum 3l_{ik}l_{ik}A_k, \tag{4}$$

where $l_{x,k}$, $l_{y,k}$, $l_{z,k}$ are the direction cosines of the axis of bonding orbital k. The sum here is simply over the bonds from the site in question to adjoining atoms from which unpaired electrons are transmitted.

The angular dependence of the shift in resonance frequency from γH_0 when the effect of dipole sum and hyperfine interaction is small compared with H_0, as it is in the paramagnetic state, for $\mathbf{H}_0$ in the xy plane, for example, is

$$\Delta\omega=\gamma\langle\mu\rangle[(D^{xx}+\kappa A^{xx})\cos^2\theta+2(D^{xy}+\kappa A^{xy})\cos\theta\sin\theta+(D^{yy}+\kappa A^{yy})\sin^2\theta+\kappa A^s], \tag{5}$$

where θ is the angle between $\mathbf{H}_0$ and the x axis. This can be written as

$$\Delta\omega=\gamma\langle\mu\rangle\{[\tfrac{1}{4}(D^{xx}+\kappa A^{xx}-D^{yy}-\kappa A^{yy})^2+(D^{xy}+\kappa A^{xy})^2]^{1/2}\cos2(\theta-\theta_{\max})-\tfrac{1}{2}D^{zz}-\tfrac{1}{2}\kappa A^{zz}+\kappa A^s\}, \tag{6}$$

where

$$\tan2\theta_{\max}=2(D^{xy}+\kappa A^{xy})\times(D^{xx}+\kappa A^{xx}-D^{yy}-\kappa A^{yy})^{-1}. \tag{7}$$

This is a $\cos2\theta$ curve with a maximum at $\theta=\theta_{\max}$ whose center is shifted $\gamma\langle\mu\rangle(\kappa A^s-\frac{1}{2}D^{zz}-\frac{1}{2}\kappa A^{zz})$ from γH_0. Thus, since the trace of the **A** tensor is zero, if the six components of **D** are known from a dipole sum calculation, A^s and the six components of the **A** tensor can be found from the patterns observed as $\mathbf{H}_0$ is rotated in the xy, xz, and yz planes. Figure 3 illustrates a resonance following this pattern. We define the tensor **E** by

$$E^{ij}=D^{ij}+\kappa A^{ij}. \tag{8}$$

It is this tensor whose elements are determined experimentally.

The experimentally determined value of A^s can be used to calculate the amount of unpaired s electron on the nonmagnetic ion if the reasonable assumption is made that this electron belongs to the valence shell. [*Note added in proof.* R. E. Watson and A. J. Freeman, Phys. Rev. Letters **6**, 343 (1961) and W. Marshall and R. Stuart, Phys. Rev. **123**, 2048 (1961) suggest that 1s electrons contribute appreciably (via a cross term with 2s electrons) to the isotropic hyperfine interactions on the F^- ions in manganese fluorides. The question of whether the isotropic shifts found in the present work arise in part from s electrons not in the valence shell affects none of the principal arguments in this paper (the precise values of the amounts of unpaired s electrons on the magnetic ions being relatively unimportant to these arguments).] An independent value of A_{ns} the hyperfine interaction per unpaired electron in state ns is required. For electrons in other than s states the problem is more complicated. Equations (4) involving the experimentally determined A^{ii}'s and A^{ij}'s and the geometrical factors known from the structure can be solved for the A_k's if the number of nonidentical bonding orbitals does not exceed the number of independent A^{ii}'s and A^{ij}'s (five at most). The A_k's thus determined are used in conjunction with appropriate values of A_{nl} to arrive at the amount of electron in state nl present on the nonmagnetic ion. The values of A_{nl} (per single unpaired electron) used are given in Table I. The A's obtained from the NMR data are referred to $\langle\mu\rangle$ the average moment of the Mn ion. Thus, since the Mn ion has five

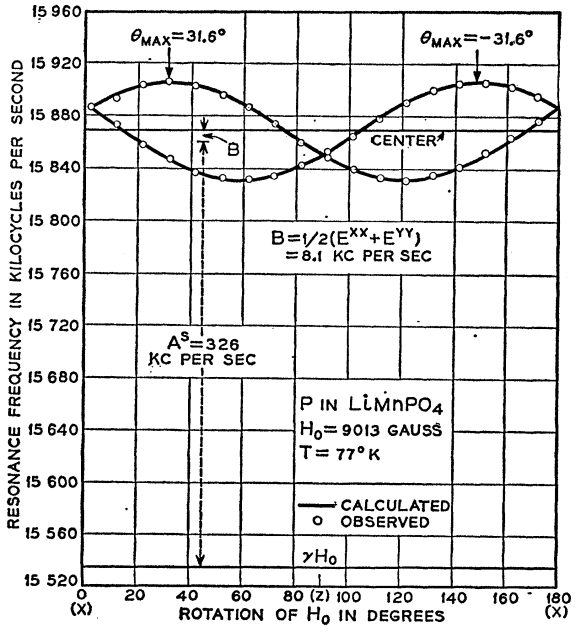

FIG. 3. Resonance frequency of P^{31} in $LiMnPO_4$ as a function of angle for rotation of $\mathbf{H}_0$ in xz plane. Symbols used are discussed in Sec. 3.

[11] C. Kittel, *Introduction to Solid-State Physics* (John Wiley & Sons, Inc., New York, 1956), 2nd ed., p. 571.

TABLE I. Hyperfine interaction constants used in this work. The values are for a single unpaired electron in the state indicated. Units are cm^{-1} and must be multiplied by $hc(=1.9861\times10^{-16}$ erg cm) to give ergs for comparison with the A's of Eq. (1) *et seq.*

Li	P
$A_{2s}=0.0134$[a]	$A_{3s}=0.564$[b]
$A_{2p}=0.0001$[c]	$A_{3p}=0.010$[c]

[a] *Landholt-Börstein Tabellen*, edited by Hans Heinrich Landholt (Springer-Verlag, Berlin, 1952), Vol. 1, Sec. 5, p. 5.
[b] Calculated using $A_{3s}=(8/3)\pi g\beta\gamma\hbar|\Psi(0)|_{3s}^2$, [T. Moriya, Progr. Theoret. Phys. (Kyoto) **16**, 23 (1956)]. $\Psi^2(0)$ is approximated using $\Psi^2(0)=Z_iZ_0^{-1}(\pi a_H^3)^{-1}(R/T)^{-3/2}$. [M. F. Crawford and A. L. Schawlow, Phys. Rev. **76**, 1310 (1949)] where the term value $T=4.694\times10^5$ cm^{-1} is taken as the average of the ground levels of PIV and PV. [*Atomic Energy Levels*, edited by C. E. Moore NBS Circular 467 (U. S. Gov't. Printing Office, Washington, D. C., 1949), Vol. I]. Z_i is taken as 15, Z_0 as ~4.5.
[c] Calculated using $A_{np}=\frac{2}{5}g\beta\gamma\hbar\langle 1/r^3\rangle_{np}$ [T. Moriya, Progr. Theoret. Phys. (Kyoto) **16**, 23 (1956).] Values of $\langle 1/r^3\rangle_{np}$ obtained from R. G. Barnes and W. V. Smith, Phys. Rev. **93**, 95 (1954).

unpaired electrons the ratio A^s/A_{3s}, for example, gives not the fraction f of a single unpaired electron present but the fraction of five electrons. Therefore $f=2SA^s/A_{3s}$ where $2S$ is the number of unpaired electrons on the magnetic ion.

Li^7 Resonances

The Li^7 resonance is complicated by the quadrupole moment of the Li^7 nucleus. However, the splittings are of the order of 10 kc/sec while the NMR (Zeeman) splittings are of order 10 Mc/sec and thus first-order perturbation theory[12] applies, and the central of the three quadrupole components can be taken as unshifted by quadrupole effects. The four crystallographically equivalent lithium atoms in the unit cell are related to one another by reflections in the xy, xz, and yz planes.[13] Two of the sites have a positive D^{xy} and two a negative and similarly for D^{xz} and D^{yz}. Thus, if $\mathbf{H}_0$ is rotated in any one of these planes the resonance of two of the sites will follow a $\cos2(\theta-|\theta_{\max}|)$ curve and the resonance of the other two will follow a $\cos2(\theta+|\theta_{\max}|)$ curve, [cf., Eq. (6)]. The two outer quadrupole components lie symmetrically to the right and left of the central component, separated from it by an amount[14]

$$\Delta\nu=eQ\mathbf{\Phi}\cdot\mathbf{H}/2hH, \tag{9}$$

where Q is the quadrupole moment and $\mathbf{H}$ the magnetic field. The tensor $\mathbf{\Phi}$, proportional to the electric field gradient, involves sums of the same sort as the dipole sum[15] and, hence, the quadrupole splitting does not destroy the twofold degeneracy of the dipole-shifted nuclear resonances. That is to say each of the two Li resonances is simply split into three components by the quadrupole interaction. In Fig. 4 are shown recorder traces of Li^7 NMR absorption for two different orientations of $\mathbf{H}_0$ in the xy plane. The parameters obtained from rotation patterns in xy, xz, and yz planes are given in the first column of Table II. Figure 5 shows the theoretical patterns for $\mathbf{H}_0$ in the xy plane calculated with the experimentally determined parameters. The procedure followed in determining these parameters will not be described. Suffice it to say that experimental traces agree well with the theoretical fit and, thus, it seems clear that the Shulman-Jaccarino picture applies to the present system. The overlapping of the patterns complicated the analysis considerably. The dipolar shifts are a function of H_0, whereas the quadrupole splittings are not. Therefore, the two patterns could have been disentangled if the frequency range of the spectrometer had been greater and thus allowed observation of the resonances at a higher H_0.

The second column of Table II shows the calculated elements of the dipole sum tensor at Li in $LiMnPO_4$ arising from the Mn atoms. It is seen that the discrepancies (given in the third column) are of the order of 5% or more (column four), whereas the experimental errors arising from susceptibility (cf. Appendix A) and structure determinations should be of the order of 1%. In order to account for this discrepancy we consider what appear to be the only two possible causes. The

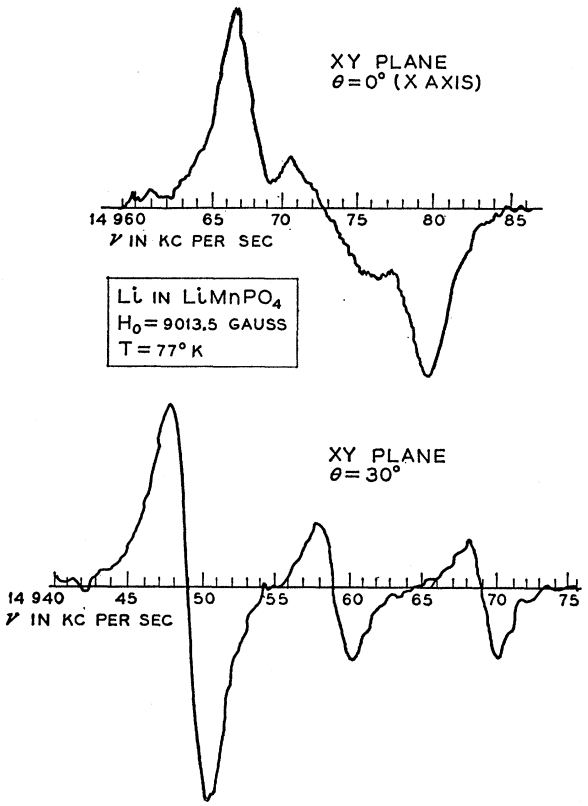

FIG. 4. Recorder traces of Li^7 NMR (absorption) in $LiMnPO_4$. Undisplaced frequency for Li^7 is 14 914.8 kc/sec. Traces are to be compared with theoretical fit in Fig. 5.

[12] Reference 1, p. 206.
[13] All structural information used in this paper is taken from Geller and Durand (reference 7). However, whereas those authors use the convention $b>a>c$, in the present paper the convention $a>b>c$ used by Byström (reference 6) is used. In general, x, y, z are used instead of a, b, c.
[14] G. M. Volkoff, H. E. Petch, and D. W. L. Smellie, Can. J. Phys. **30**, 270 (1952).
[15] R. Bersohn, J. Chem. Phys. **29**, 326 (1958).

TABLE II. Elements of tensors (in Å^{-3}) for Li in $LiMnPO_4$.

	Experimental[a]	Calculated D^{ij} due to Mn	Residue	Residue / Calculated	Calculated[b,c] D^{ij} due to O[b]		
					O^1	O^2	O^3
E^{xx}	+0.0708	+0.0739	−0.0031	0.042	−0.0786	−0.2070	+0.1836
E^{yy}	−0.0437	−0.0429	+0.0008	0.018	+0.0664	+0.1130	−0.1796
E^{zz}	−0.0271	−0.0310	+0.0039	0.126	+0.0120	+0.0940	−0.0040
E^{xy}	±0.0073	+0.0061	0.0012	0.20	−0.1582	+0.0952	−0.0742
E^{xz}	±0.0043	+0.0032	0.0011	0.34	+0.1184	+0.0776	−0.2446
E^s	0.0046	−0.0064	0.0018	0.28	−0.1822	+0.2596	+0.0578
κA^s	0.0025						

Quadrupole (kc/sec)

Φ^{xx}	−10.6	$\Phi^{xy}=-10.8$	
Φ^{yy}	−10.6	$\Phi^{xz}=-28.4$	
Φ^{zz}	+21.2	$\Phi^{yz}=+28.4$	

[a] cf. Appendix A.
[b] Signs of off-diagonal elements are those for Li at (0,0,0).
[c] These figures are purely geometrical and must be multiplied by $f\langle\mu\rangle$, where f is the fraction of the total magnetism assigned to the type of oxygen in question. The $\langle\mu\rangle$ for Mn must be reduced to take account of any such shift of magnetism.

first possibility is that the discrepancy arises wholly or in part from hyperfine interaction of the Li^7 nucleus with unpaired electrons having p character. This possibility seems definitely excluded by the smallness of the observed A^s. (This quantity, which is barely above experimental error, sets an upper limit of about 0.1% of an unpaired s electron on the Li ion or 0.017/Mn–O–Li linkage.) As is shown in Table I, the hyperfine interaction constant for $2p$ electrons on Li is expected to be two orders of magnitude smaller than that of $2s$ electrons. We expect the amount of $2p$ electron involved in octahedral bonds to be only about three times the amount of $2s$ electron. Hence, the expected effect of $2p$ hyperfine interaction comes out to be at most about a percent or two of the observed *discrepancy* and thus is negligible. The second possibility is that it is erroneous to take the observed paramagnetism as localized completely on the manganese ions and that, in fact, an appreciable fraction of the unpaired electrons resides on the oxygen atoms. In MnF_2 it was found that the amount of unpaired $2s$ and $2p$ electron localized on the fluorine ion was of the order of several percent. On the basis of electronegativity differences the Mn–O bond would be expected to have at least as much covalent character as the Mn–F bond. Thus, one would not be surprised at several percent of unpaired electron on the oxygen atoms.

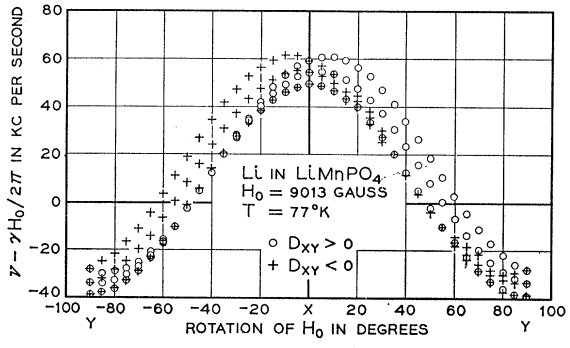

FIG. 5. Theoretical fit to observed Li^7 NMR in $LiMnPO_4$ with $\mathbf{H}_0$ in xy plane. Constants used are shown in Table II. At a given angle the crosses give the position of the three quadrupole components of the NMR of two of the Li sites in the unit cell and the circles give the position for the other two sites. Note that the splitting out of the two satellites given by Eq. (9) is zero for some angle and the three components are then superimposed. Observed resonances for $\theta=0°$ and $\theta=30°$ are shown in Fig. 4.

The oxygen atoms lie in three crystallographically different sites. The six oxygens arranged in a distorted octahedron around each manganese comprise one type 1, one type 2, and four type 3 oxygens.[7] The Mn–O distances are given in Table III. Each type 1 and type 2 oxygen belongs to only one MnO_6 octahedron while each type 3 oxygen belongs to two such octahedra and is connected to the two central manganese atoms by bonds of different length. The dipole sums at Li for magnetism on the three types of oxygen have been calculated and are shown in Table II. If we let f_1, f_2, and $2f_3$ represent the fraction of the total magnetism transferred to an oxygen of each of the three types, the fraction of magnetism left on each Mn will be $1-f_1-f_2-4f_3$. Using the calculated dipole sums at lithium due to magnetism on oxygens and manganese, making use of (2), together with the experimental E^{ij}'s it is theoretically possible to calculate f_1, f_2, and f_3. However, we are dealing with the differences $(E^{ij}-D^{ij})$ of large numbers, and the errors in these differences could be of the order of 10 or 20%. A check of the effect of such errors on the calculated f's showed that these experi-

TABLE III. Internuclear distances and angles in phosphate tetrahedra and associated manganese atoms.[a] Manganese designations refer to Fig. 8.

Manganese	Oxygen	Mn–O	P–O	∠Mn–O–P
Mn^A	O^2	2.139 Å	1.526 Å	128°
Mn^B, Mn^D	O^3	2.130	1.547	130°
Mn^C	O^1	2.240	1.545	122°
Mn^E	O^3	2.283	1.547	95°

[a] See reference 7.

TABLE IV. Elements of tensors (in Å^{-3}) for P in $LiMnPO_4$.

	Experimental[a]	Calculated[b] D^{ij} due to Mn	Residue	Residue / Calculated	Calculated[b,c] D^{ij} due to Oxygen		
					O^1	O^2	O^3
E^{xx}	+0.0311	+0.0400	−0.0089	0.22	−0.2895	+0.4200	−0.1570
E^{yy}	−0.0202	−0.0203	+0.0001	0.005	−0.2629	−0.2383	+0.4448
E^{zz}	−0.0109	−0.0197	+0.0088	0.045	+0.5522	−0.1818	−0.2878
E^{xy}	0.0	0.0	0.0	0.0	0.0	0.0	0.0
E^{xz}	±0.0416	−0.0377	0.0039	0.10	+0.0242	+0.2668	−0.2934
E^{yz}	0.0	0.0	0.0	0.0	0.0	0.0	0.0
κA[a]	+0.408						

[a] cf. Appendix A.
[b] Signs of off-diagonal elements are those for P^1 (see reference 19).
[c] These figures are purely geometrical and must be multiplied by $f\langle\mu\rangle$, where f is the fraction of the total magnetism assigned to the type of oxygen in question. The $\langle\mu\rangle$ for Mn must be reduced to take account of any such shift of magnetism.

mental errors could easily lead to errors of the same order as the f's themselves. This great unreliability is further complicated by an ambiguity in sign of the off-diagonal E^{ij}'s. The result is that direct solution of the equations is no help even in establishing the order of magnitude of the f's. However, we can arrive at such an order of magnitude by making the reasonable assumption that each of the six Mn–O bonds transmits roughly the same amount of magnetism to the oxygen. On this assumption ($f_1=f_2=f_3=f$) each of the E's gives us a value of f and these values are relatively less sensitive to experimental errors and to errors arising from differences in the individual f's. Solving the equations for E^{xx} and E^{zz}

$$\begin{aligned} D_{\mathrm{Mn}}{}^{xx}(1-6f)+(D_{01}{}^{xx}+D_{02}{}^{xx}+2D_{03}{}^{xx})f&=E_{\exp}{}^{xx} \\ D_{\mathrm{Mn}}{}^{zz}(1-6f)+(D_{01}{}^{zz}+D_{02}{}^{zz}+2D_{03}{}^{zz})f&=E_{\exp}{}^{zz} \end{aligned} \tag{10}$$

for which the discrepancies are largest, gives values $f=0.009$ and 0.014, respectively, using the numbers in Table II. These results are consistent with one another and with the estimate that f is the order of one or two percent. In this picture each Mn ion has transmitted a total of perhaps five or ten percent of its magnetism to the surrounding oxygens.

P^{31} Resonances

The P^{31} nucleus has a spin of $\frac{1}{2}$; hence, there is no quadrupole splitting of the NMR spectrum. There are four crystallographically equivalent phosphorus sites in the unit cell. The xz plane is a mirror plane for these sites and, thus, the y axis is a principal axis of the **D** and **A** tensors and $D^{xy}=A^{xy}=D^{yz}=A^{yz}=0$. A single resonance with $\theta_{\max}=0$ is therefore expected for $\mathbf{H}_0$ in xy, yz planes and two resonances are possible in the xz plane. The observed patterns are as expected. The parameters obtained from rotation patterns in xy, xz, and yz planes are given in the first column of Table IV. Figure 3 shows experimental points in the xz plane and the fit made with (6). The isotropic shift of 326 kc/sec is quite striking and unequivocal as compared with that of the Li resonances. This shift corresponds about 0.4% of an unpaired $3s$ electron on the phosphorus atom.

The second column of Table IV shows the calculated elements of the dipole sum tensor at phosphorus on the assumption that all the magnetism is on the Mn atoms. We see that the discrepancy (third column) is considerable. The large isotropic shift observed prevents us from ruling out anisotropic shifts due to hyperfine interaction of phosphorus electrons as we were able to do in the case of the Li resonances. If we had been able to arrive at precise values of the distribution of magnetism on the oxygen atoms by analysis of the Li spectra we should be able to correct the dipole sum at phosphorus for this effect and then take the residual discrepancy as arising from hyperfine interaction of unpaired $3p$ phosphorus electrons with the phosphorus nucleus. However, we were able to arrive only at a rough estimate of the distribution of magnetism on the oxygen atoms and the uncertainties in any use of these estimates to correct the dipole sum at phosphorus are much too great to make it meaningful. We can, however, see whether a reasonable distribution of charge could account for the discrepancies as it could in the case of Li. A calculation similar to that carried out for Li gives for E^{xx} and E^{zz}, for which the discrepancies are largest, the values $f=+0.021$ and -0.100, in contrast with the reasonableness and consistency of values obtained for Li. We conclude from this that it is difficult to account for the discrepancy in the angular behavior of the phosphorus NMR solely on the basis of magnetism transferred to the oxygens and that it is therefore likely that there are uncompensated p electrons on the phosphorus atoms. This matter will be discussed further below. It has been estimated that each of the four P–O linkages in phosphates has of the order of 0.5 of a π bond involving $3d$ electrons of the phosphorus atom.[16] However, $3d$ electrons are considerably less penetrating[17] than $3p$ and, hence, we should expect their hyperfine interaction to be small compared with that of the $3p$ electrons.

For $\mathbf{H}_0(=9013\ \mathrm{G})\|x$ the shift of the phosphorus

[16] J. R. van Wazer, *Phosphorus and Its Compounds* (Interscience Publishers, Inc., New York, 1958), Vol. 1, Chap. I.
[17] Cf., J. C. Slater, *Quantum Theory of Matter* (McGraw-Hill Book Company, Inc., New York, 1951), p. 150–156.

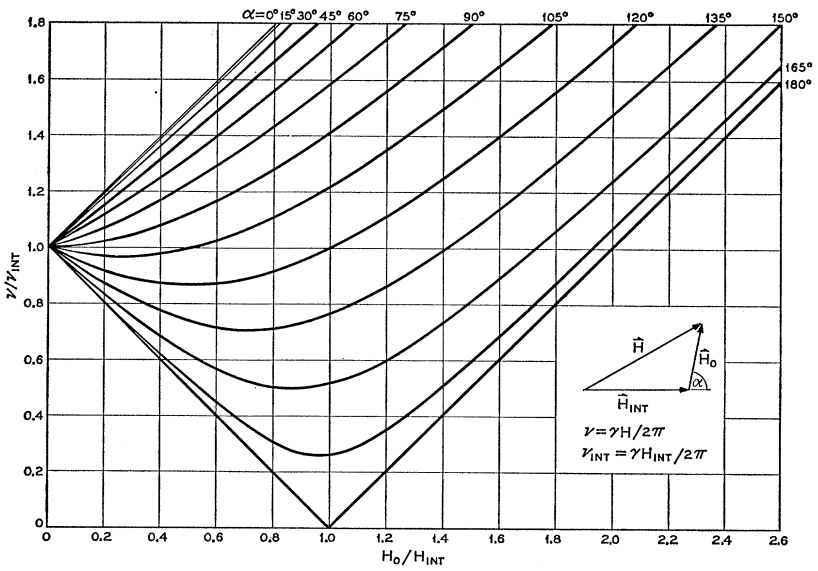

FIG. 6. Behavior of nuclear magnetic resonances in antiferromagnetic crystals as magnitude and direction of external magnetic field is varied. Cf., Eq. (11).

resonance from that of phosphorus in H_3PO_4 is 350.9 kc/sec at liquid-nitrogen temperature and 142.2 kc/sec at ~300°K. The ratio of these shifts is 2.47. For the Li^7 resonance the shifts are 54.3 kc/sec and 21.9 kc/sec and the ratio 2.48. The ratio of measured susceptibilities at the two temperatures is 2.42. The closeness of the ratios for phosphorus and Li and the reasonable agreement with the susceptibilities indicates that the predicted proportionality of shifts to $\langle\mu\rangle$ is fulfilled.

4. RESONANCES IN THE ANTIFERROMAGNETIC STATE

Theory

In the antiferromagnetic state one can describe the expected behavior of the nuclear resonances of the lithium and phosphorus atoms in terms of an internal magnetic field vector $\mathbf{H}_{\text{int}}$ which may vary from one phosphorus or lithium atom to another in the magnetic unit cell. This field arises from the same sources as the internal fields (i.e., shifts) in the paramagnetic state but differs from these shifts in that the electron spins do not in general line up with $\mathbf{H}_0$ as they do in the paramagnetic state but have a direction fixed in the crystal lattice. H_{int} may be rather large, particularly well below the Néel temperature, because the magnetic moment of Mn approaches 5 Bohr magnetons as compared for example with 0.05 Bohr magnetons for the same ion in $LiMnPO_4$ in the paramagnetic state at 77°K and $H_0=9$ kG.

It is easily seen from the small diagram in Fig. 6 that for a single crystal

$$\nu(T)=\gamma H/2\pi=\gamma(H_{\text{int}}^2+2H_{\text{int}}H_0\cos\alpha+H_0^2)^{1/2}/2\pi, \tag{11}$$

where ν is the resonance frequency, and α the angle between $\mathbf{H}_0$ and $\mathbf{H}_{\text{int}}(T)$. This equation assumes that H_{int} is not a function of H_0 and thus ignores the small susceptibility of the two sublattices. H_{int} is, of course, a function of temperature, being proportional to $M(T)$ the (temperature-dependent) sublattice magnetization. Figure 6 shows plots of $2\pi\nu/\gamma H_{\text{int}}$ versus H_0/H_{int} for various values of α. Experimentally, once the pattern is clear two points suffice to establish H_{int} and α for each curve; a third point allows γ and thus the identity of the nucleus to be established. Measurement of α for three directions of $\mathbf{H}_0$ not lying in a plane uniquely specifies the direction of $\mathbf{H}_{\text{int}}$.

The susceptibility in the antiferromagnetic state is no longer isotropic, that for $\mathbf{H}_0$ parallel to the lined up spins $\chi_{\parallel}$ being considerably smaller than $\chi_{\perp}$ well below the Néel temperature. In the present case[18] $\chi_{\text{para}}^{77°K}$ lies between $\chi_{\perp}^{4.2°K}$ and $\chi_{\parallel}^{3.2°K}$. Thus, there is expected a small angle-dependent shift from the frequencies given in Eq. (11), differing in magnitude from those in the paramagnetic state in accordance with the different susceptibilities. Because the susceptibility is no longer isotropic, the shift arising from A^s now has an angular dependence. In general the directions of both $\mathbf{H}_{\text{int}}$ and of the small $\mathbf{H}$ due to the susceptibility will be different for the different crystallographically equivalent sites and each such site must be treated separately.

As we shall see below, predicting $\mathbf{H}_{\text{int}}$ for Li and phosphorus in antiferromagnetic $LiMnPO_4$, even at helium temperatures where one can assume virtually complete lining up of electron spins requires much more information that is available from the paramagnetic measurements. A good way to start a search is to set the spectrometer at its maximum frequency and sweep H_0 from near zero to its maximum. The two maxima in the present case are 16 Mc/sec and 16 kG. This allows one to see resonances of the type shown in Fig. 6 which have zero-field resonances both above and below 16

[18] R. M. Bozorth (private communication).

Mc/sec. Details of the considerations that determine the conditions for seeing a resonance of given $\mathbf{H}_{\text{int}}$ are given in Appendix B.

Li^7 and P^{31} Resonances

At 4.2°K the Li resonance in pure $LiMnPO_4$ is found to be essentially unshifted from γH_0, which is to say

$$H_{\text{int}}{}^{\text{Li}}=0.$$

Four phosphorus resonances are observed, each with

$$H_{\text{int}}{}^{\text{P}}=4408\pm 2 \text{ G},$$

but corresponding to two different directions of alignment of this vector (actually four—positive and negative along each of the two directions) as shown in the small diagram of Fig. 7. At the time these phosphorus resonances were first observed the only information available on the direction of antiferromagnetic alignment in $LiMnPO_4$ was the magnetic susceptibility measurement of Bozorth and Kramer[8] on a mineral sample $LiMn_{0.7}Fe_{0.3}PO_4$ which showed the alignment to be along the y axis. We have seen that the **D** and **A** tensors have one principal axis along the y direction in the crystal, and thus for spins parallel to the y direction we should expect the field at phosphorus also to be parallel to the y direction. The observed presence of two directions of $\mathbf{H}_{\text{int}}$ is what one would predict for spins aligned along some direction in the xz plane, the two resonances arising from positive and negative values of the nonvanishing $D^{xz}+\kappa A^{xz}$ (cf., Sec. 6).

Subsequent susceptibility measurements by Bozorth[18] showed that χ along the x axis in pure $LiMnPO_4$ approaches a value close to zero at 0°K and hence that the *individual* manganese spins are closely parallel to the x axis. This was substantiated by the extremely small shift of the Li resonance at 4.2°K for $\mathbf{H}_0$ along the x axis described in the next paragraph.

The Li resonance at 4.2°K is, as has been said above, essentially unshifted from γH_0. Small shifts and splittings observed are roughly consistent with experimental susceptibilities and the previously determined quadrupole behavior in the paramagnetic state. With $\mathbf{H}_0$ (=9669 G)$\|x$ the resonance is similar in structure to the one observed in the paramagnetic state for the same orientation of $\mathbf{H}_0$ and is shifted 2.5 kc/sec from γH_0. The shift of 2.5 kc/sec gives $\chi_{\|}{}^{4.2°\text{K}}/\chi^{77.3°\text{K}}=0.05$ as compared with a value of 0.12 obtained by direct susceptibility measurements.[18] With $\mathbf{H}_0$(=9669 G)$\|z$ three quadrupole components are resolved with a total splitting of 20.2 kc/sec as compared with 21.2 kc/sec observed in the paramagnetic state. The resonance was shifted an amount (−23.7 kc/sec) which gives $\chi_{\perp}{}^{4.2°\text{K}}/\chi^{77.3°\text{K}}=1.3$ as compared with 1.4 from direct susceptibility measurements.[18]

The Li resonance was followed in temperature from 20 to 50°K by allowing the cryostat to warm up from the temperature of liquid hydrogen. The Varian magnet was swept by a 5-sec sawtooth voltage from a Hewlett-Packard 130B oscilloscope (the large dc bias of the sawtooth was bucked by dry cell batteries). The Li resonance was displayed on a strip chart recorder. The resonance was sharp and essentially unshifted from γH_0 over the entire temperature range. At 34.85±0.1°K, as measured on a calibrated thermocouple, there was a relatively sharp discontinuity in the resonance, the height increasing by about a third as the temperature was passed from below. No other discontinuity was observed in the range 20–50°K. The width of the resonance remained apparently unchanged. This discontinuity is taken to arise from the transition from antiferromagnetic-to-paramagnetic state. Thus, the Néel temperature is taken to be 34.85±0.1°K, which agrees with a less precise susceptibility measurement by Bozorth.[18]

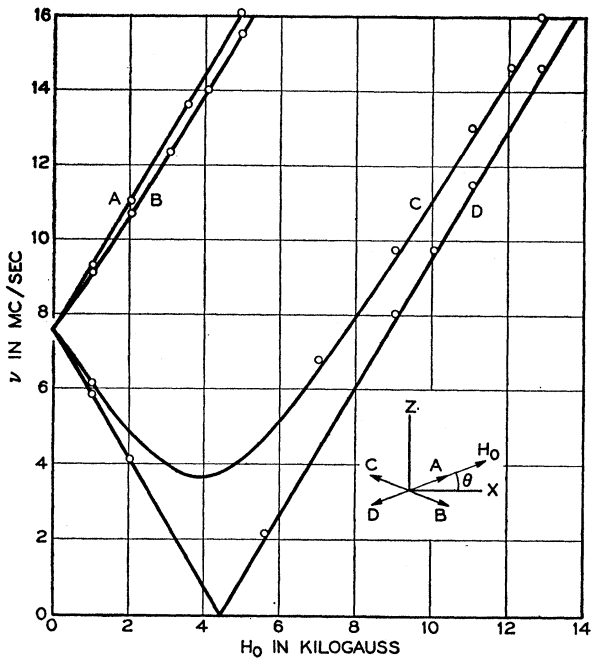

FIG. 7. Resonance frequency of P^{31} in antiferromagnetic $LiMnPO_4$ at 4.2°K as a function of H_0. Inset shows roughly the directions of $\mathbf{H}_0$ and of $\mathbf{H}_{\text{int}}$ at the four phosphorus sites in the unit cell relative to the crystallographic axes. For branches A and D the lines are a plot of Eq. (11) for $\alpha=0$. For branches B and C the solid lines are a plot of (11) for $\alpha=29°$ ($\theta=14.5°$). See text for further discussion.

Measurements of the P^{31} resonances at 4.2°K are shown in Fig. 7. It is seen that the experimental points follow the theoretical curves fitted from (11) fairly well. Directions of the two alignments of $\mathbf{H}_{\text{int}}$ in the xz plane were first measured as ±14°±0.5° from the x axis by fixing H_0 in the neighborhood of 13 kG and plotting the resonance frequencies as a function of rotation in the xz plane. According to Eq. (11) minima would occur when $\mathbf{H}_0$ is aligned with $\mathbf{H}_{\text{int}}$. Minima were found to occur at ±13° from the axis. Calculation shows that a shift of ~1° toward the x axis is introduced by the effect of susceptibility ignored in Eq. (11). The best

fit (taking into account the effect of susceptibility) of the field dependence of the resonances under the conditions described in Fig. 7 is for a value of 14.5° for this angle. The agreement between these two ways of arriving at the alignment of $\mathbf{H}_{\text{int}}$ is thus seen to be good.

Interpretation of the phosphorus reasonances in the antiferromagnetic state is much more complicated than that of the Li resonance. It was not possible to break up the observed anisotropy in the paramagnetic state into the contributions from dipolar fields due to magnetism on Mn and oxygen and from hyperfine interaction with the phosphorus nucleus. Further, there is no basis for breaking up the observed isotropic shift in the paramagnetic state into contributions from the five nearest neighbor Mn ions. All this information would be required to predict $\mathbf{H}_{\text{int}}{}^{\text{P}}$. However, we can draw some conclusions by examining the possible size of various effects.

The following parameters describe the observed phosphorus resonances in the antiferromagnetic state

$$E^{xx}=7.37 \text{ Mc/sec}, \quad E^{xz}=\pm 1.84 \text{ Mc/sec}, \quad E^{xy}=0,$$

where E^{xx} is now taken to include isotropic contributions from s electrons.

The off-diagonal E^{xz} is unaffected by the isotropic contributions and, hence, is easier to discuss. The sign of off-diagonal element is not determined by experiment, but the absolute value can be compared with calculation. All calculations will be for P^{I}.[19] If all the magnetism is taken as residing on the Mn atoms $E^{xz}=-2.57$ Mc/sec. The effect of transmitting 0.01 of the magnetism along each Mn–O bond (in keeping with estimates made from the Li NMR) is to change this to 2.19 Mc/sec which is not out of line with the experimental ± 1.84 Mc/sec.

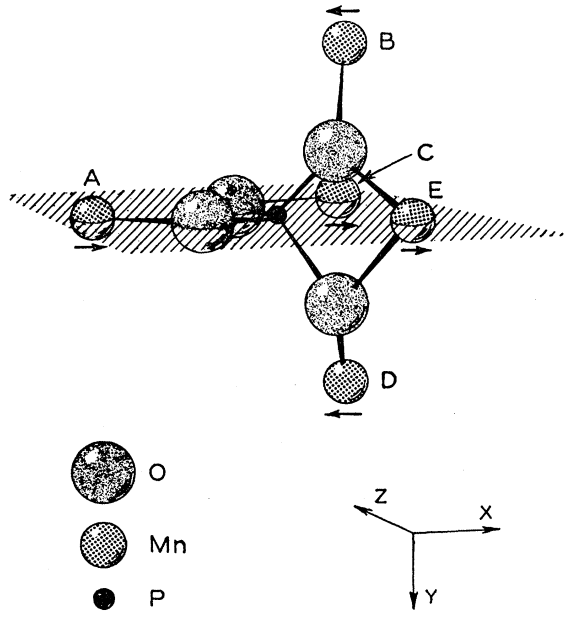

FIG. 8. The arrangement of oxygen and manganese atoms around P^{I}. Arrows give directions and relative senses of electron spins in antiferromagnetic state.

[19] P^{I} is used to designate the P atom at position $(x,\frac{1}{4},z)$ using the convention $a>b>c$ (cf., reference 13).

Figure 8 shows the arrangement of oxygen and manganese atoms around P^{I} and relative spin directions in the antiferromagnetic state (cf., Sec. 6). The internuclear distances and P–O–Mn angles are given in Table III. Four of the Mn atoms (A,B,C,D) are "connected" to the phosphorus atom by similar Mn–O–P paths with angles of 122–130°. The fifth Mn atom is unique in that it is closer to the phosphorus atom and is "connected" by two oxygen atoms with Mn–O–P angle of 95°. Typical O–P–O angles are 107°, 113° and 103°, close to the tetrahedral angle of 109.5°. The question of transmission of uncompensated spin around a 95° "corner" is discussed below. For the present we give predicted figures for the cases where such transmission does not occur and the case where it does. In the former case each of the four O-P bonds is assigned an equal contribution. In the latter the two O–P bonds involved in the 95° Mn–O–P path are assigned a double contribution (one from Mn^{B} and one from Mn^{E}).

One percent of an unpaired p electron transmitted to the phosphorus atom from each of the four O–P bonds would result, by hyperfine interaction, in a reversal of sign of E^{xz} to $+1.11$ Mc/sec, again comparable to the experimental ± 1.84 Mc/sec (1.22% would give exactly $+1.84$ Mc/sec). Full contribution from Mn^{E} would give $E^{xz}=2.77$ Mc/sec (0.81% from each bond would give the experimental 1.84 Mc/sec). The experimental value of E^{xz} is thus consistent with either no unpaired p electron on the phosphorus atom or about 1% per bond. The question of the effect of Mn^{E} is left unsettled.

We now consider E^{xx}. If all the magnetism is taken to reside on the Mn atoms and the effect of unpaired s electrons on phosphorus is neglected for the moment $E^{xx}=7.51$ Mc/sec. The effect of transmitting 0.01 of the magnetism along each Mn–O bond is to change this to 7.25 Mc/sec, still in rather good agreement with the experimental 7.37 Mc/sec. One percent of a p electron from each O–P bond would raise this by hyperfine interaction to 9.66 Mc/sec. Full contribution from Mn^{E} would make E^{xx} more positive by about 1.10 Mc/sec. Whereas the presence of unpaired p electrons on the phosphorus atoms was not firmly established in the paramagnetic state, the large isotropic shift demonstrated the presence of unpaired s electrons. In the antiferromagnetic state if we assume for the moment no transmission of s electrons along the 95° Mn–O–P paths it is seen from Fig. 8 that of the remaining four O–Mn–O paths two will be transmitting up spins and two down spins, and if all four paths were identical there would be no net effect due to these s electrons. If these four paths were identical and the

fifth path(s) were only some fraction, f effective, compared with each of the other four E^{xx} for P^I would become more positive by $\sim 7.00f$ Mc/sec thus increasing the discrepancy with experiment. Indeed, seemingly the only factor which might reduce the calculated E^{xx} (for P^I) is that the angle Mn–O–P is greatest for Mn^B and Mn^D and the sum of the P–O and Mn–O distances is on the whole somewhat smaller for these two atoms. It seems unlikely that this effect would be large enough to cancel any sizable s electron contribution from Mn^E. We conclude then that the 95° Mn–O–P angle reduces considerably the transmission of unpaired electrons into the s orbitals of phosphorus. The question of the presence of unpaired p electrons on the phosphorus atom is left undecided as is the contribution of the 95° Mn–O–P path to p electrons on phosphorus. The angular pattern of the phosphorus NMR in the paramagnetic state is, as has been seen in Sec. 3, not easily explained on the basis of a reasonable distribution of the magnetism between Mn and O atoms and thus seems to require the presence of unpaired p electrons on phosphorus. Experimental values of E^{xx} and E^{xz} for phosphorus in the antiferromagnetic state agree well with a picture in which about 0.01 of the magnetism is transferred to oxygen along each Mn–O bond (as estimated from paramagnetic Li NMR), no unpaired electrons are transferred to s orbitals of phosphorus along the 95° paths, the remaining Mn–O–P paths transmit equal amounts of unpaired electrons of up and down spin into s orbitals, and no unpaired p electron is present on phosphorus. The possibility that some balance exists between the positive effects of transmission of unpaired spins into p and s orbitals along the 95° paths and the negative effect of less transmission into s orbitals along longer and more acute Mn–O–P paths is not ruled out.

5. DISCUSSION OF RESONANCE SHIFTS

It has been definitely established in Sec. 3 that there is $\sim 0.4\%$ of an unpaired electron in the $3s$ orbital of the phosphorus atom and $\leq 0.1\%$ of an unpaired electron in the $2s$ orbital of the Li atom in paramagnetic $LiMnPO_4$. There is also good evidence (Sec. 4) for the fact that the transmission of these unpaired electrons is much smaller along the other three paths where the angles are 122–130°. Previous work with fluorine compounds has, as we know, established that uncompensated electron spins are introduced into valence orbitals of neighboring nonmagnetic ions from magnetic ions by covalent bonding and overlap effects.[2,20]

We consider the upper right-hand oxygen atom in Fig. 8. There is a relatively strongly covalent bond between this oxygen and the phosphorus.[16] The orbitals involved in the σ bond are probably sp^3 for phosphorus and a p orbital (say p_z) for oxygen.[16,21] We expect Mn–O covalent bonds of the order of a percent or more, similar to the Mn–F bonds in MnF_2,[2] to be formed with Mn^B and Mn^E. Since O–Mn^E is nearly at right angles to O–P we expect one of the remaining two p orbitals (say p_y) of oxygen to point toward Mn^E and participate in the bond. The bond Mn^B would involve the p_z as well as p_x and p_y. Hence, we should expect some unpaired p_z electron introduced by Mn^B to produce uncompensated p and s electrons at phosphorus in the usual manner through the O–P bond. In contrast the O–Mn^E bond, involving virtually pure p_y, should have no such effect on phosphorus. We have neglected the s electrons on the oxygen as a transmitter of unpaired electrons from Mn to phosphorus. Shulman and Knox[22] have shown in $KNiF_3$, for example, that the fraction of an unpaired s electron on fluorine is an order of magnitude less than the fraction of an unpaired p electron on fluorine. Further, there are two bonds, the Mn-O and the O–P, involved, and the relative attenuation of the effect for s as compared with p electrons will then be the product of the attenuations in the two bonds or over all probably at least an order of magnitude.

The effect of π-like overlaps of the sort discussed by Casselman and Keffer[23] for MnO is not as easily ruled out. The geometrical situation is almost identical for the 90° Mn–O–Mn bond angle in MnO and the 95° Mn–O–P angle in $LiMnPO_4$. In both cases, therefore, the overlap of xy-like Mn $3d$ orbitals onto the other bond (O–Mn or O–P) is similar. The principal difference is that the P–O bond is considerably more covalent than the Mn–O bond. These π overlaps are smaller for the other four Mn–O–P paths where the bond angles are 122–130° but would be similar for all four. Thus, the effects of the four paths involving, in the antiferromagnetic state, two up spins and two down should continue to cancel and the effect of the fifth manganese, if any, be uncompensated. Hence, on this qualitative picture the apparent small effectiveness of the 95° Mn–O–P path is consistent with previous pictures of superexchange as regards σ paths but not as regards π paths. (We note that Karplus[24] has discussed transmission of unpaired electrons around corners in the $H_3C\cdot$ free radical. He shows that the amount of unpaired electron finding its way to the protons increases markedly as the angle between the direction of the orbital containing the unpaired electron, taken as along the figure axis, and the C–H bond becomes greater than 90°.)

We now compare the isotropic shifts in $LiMnPO_4$ with those in MnF_2. The amount of unpaired s electron

[20] F. Keffer, T. Oguchi, W. O'Sullivan, and J. Yamashita, Phys. Rev. **115**, 1553 (1959).

[21] Designations of p orbitals here as x, y, and z are unrelated to the crystal axes shown in Fig. 8.

[22] R. G. Shulman and K. Knox, Phys. Rev. Letters, **4**, 603 (1960).

[23] T. N. Casselman and F. Keffer, Phys. Rev. Letters **4**, 498 (1960).

[24] M. Karplus, J. Chem. Phys. **30**, 15 (1959).

on the phosphorus nucleus in the paramagnetic state is 0.4%. If we ignore the 95° Mn–O–P path this represents 0.1% per Mn–O–P path. If we apply to fluorine the method of computing A_{2s} used above for phosphorus we obtain $A_{2s}{}^{F}=2.75$ cm^{-1} as compared with 1.57 cm^{-1} computed by Shulman and Jaccarino.[2] We use the former value for the sake of consistency and using Shulman's and Jaccarino's shifts get a value 0.27% unpaired s electron per Mn–F bond, or approximately three times that for Mn–O–P paths. The Mn–O bond is very similar to the Mn–F bond in MnF_2. Experimental points on the ionic-covalent character versus electronegativity difference graph[25] show very little difference in covalent character between electronegativity difference 2.5 (Mn–F) and 2.0 (Mn–O) though the smoothed curve shows Mn–O as having perhaps 1.5 times the covalency of Mn-F. Thus, one would expect the amount of unpaired electron reaching the nonmagnetic ion to be roughly the same for Mn–O and Mn–F. The factor of ~3 can be thought of as the attenuation in getting this magnetic effect around the Mn–O–P corner (122–130°) and into the p orbital. The fact that this attenuation is relatively small substantiates the idea that covalent bonding is one of the important mechanisms of transporting unpaired spin from one atom to another. The transmission is of the order of 1% along the Mn–F (and presumably Mn–O) bond where the covalency is small and of the order of tens of percent along P–O where covalency is large. A further comparison is provided by the Li and phosphorus NMR shifts in $LiMnPO_4$. The Li shifts correspond to $\leq 0.017\%$ of an electron in s orbital per Mn–O–Li path or one-sixth that per Mn–O–P path. This is in keeping with the considerably smaller covalent contribution expected for the Li–O bond as compared with the P–O bond.

We should expect the factors affecting the transmission of magnetism from Mn to phosphorus along Mn–O–P paths to be essentially the same as those affecting the strength of the superexchange linkage along, say a Mn–F–Mn path. In both cases there is involved the transmission of uncompensated electron spin to an adjoining atom. In the first case the amount of unpaired spin that finds its way onto the phosphorus depends in part upon interaction between electrons in the two bonding orbitals of the oxygen atom. In the second case the strength of the superexchange depends also in part upon the interaction between electrons in the two bonding orbitals of the intervening atom. Thus, the present experiments further substantiate the idea of second nearest neighbor interactions through intervening atoms. The dependence of the transmission of spin upon bond angles and covalency for Mn–O–P and Mn–O–Li paths discussed above is, as we have seen, in agreement with the predictions of the theory of superexchange regarding the strength of the superexchange interaction.[3,4]

6. ANTIFERROMAGNETIC ARRANGEMENT

Determination

The value of H_{int} for the Li resonances at 4.2°K and the number and symmetry of Li and phosphorus resonances observed, when combined with the susceptibility data, allow us to deduce the arrangement of spins in the antiferromagnetic state. We have said that the susceptibility data, confirmed by the behavior of the Li resonance, show the Mn spins to be aligned parallel and antiparallel to the x axis. There remains to be determined the arrangement of these spins in the lattice. The crystal structure has been described in Sec. 1. Figure 2 shows that each Mn is "connected" to each of four other Mn neighbors in the puckered plane through an oxygen (Mn–O–Mn angle 125°). Successive planes are separated by PO_4 tetrahedra sharing corners and edges with LiO_6 octahedra. The Mn–O–Mn linkages within the planes are conventional ones for superexchange. The presence of such two-dimensional lattices, with promising superexchange linkages, connected by PO_4 and LiO_6 groups of unknown superexchange efficacy would not make us confidently predict antiferromagnetism. However, with the presence of antiferromagnetism established, we should be very surprised if each plane were not antiferromagnetic within itself. However, we shall not neglect the possibility that they are not. The expected antiferromagnetic arrangement of spins in the plane is shown in Fig. 2.For a single plane an arrangement with each spin reversed would, of course, be equivalent. As regards the correla-

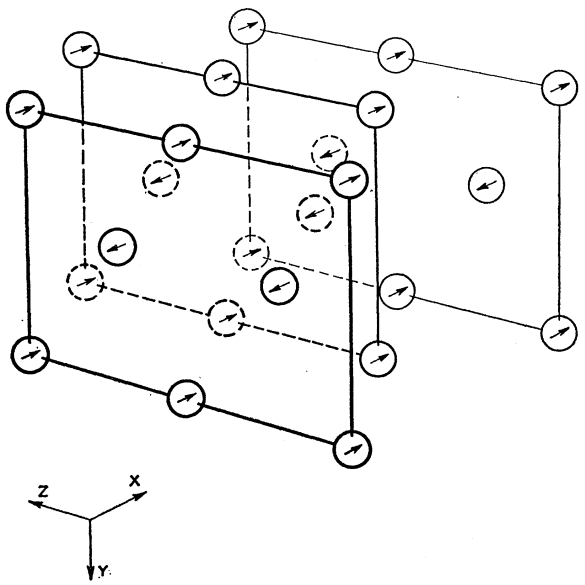

FIG. 9. Observed arrangement of spins on Mn atoms in $LiMnPO_4$ showing correlation in going from one puckered plane to next.

[25] L. Pauling, *The Nature of the Chemical Bond* (Cornell University Press, Ithaca, New York, 1960), 3rd ed., p. 99.

tion of spin arrangements in two adjoining planes there are two possibilities. The correlation can be (a) that of the front two planes in Fig. 9, or it can be (b) such that each of the spins in the second plane is reversed. Let us consider the three simplest possible patterns of correlation of antiferromagnetic planes for the whole crystal. (1) Each plane is related to its neighbors in the manner (a). This is the arrangement shown in Fig. 9. (2) Each plane is related to its neighbors in the manner (b), and (3) The relation between planes is random. The simplest arrangement with ferromagnetic planes giving rise to no net moment for the crystal is (4) Each plane is ferromagnetic within itself, and the spin direction alternates from one plane to the next.

We now determine the number of possible directions of $\mathbf{H}_{\text{int}}^{\text{Li}}$ and $\mathbf{H}_{\text{int}}^{\text{P}}$ for each of the four arrangements. Since the spins point along the x axis the field at site a can be expressed as

$$\mathbf{H}_{\text{int}}{}^{a}/\langle\mu\rangle=(E_a{}^{xx}+\kappa A_a{}^{s})\mathbf{i}+E_a{}^{xy}\mathbf{j}+E_a{}^{xz}\mathbf{k}$$

Since the four sites of, say, phosphorus are crystallographically equivalent, if the magnetic and crystallographic cells are identical, as they are for arrangements (1), (2), and (4), the coefficients of **i**, **j**, **k** will have the same magnitude for the four sites but may be of different sign. The relative signs for different sites can be obtained in a straightforward manner for a given arrangement of up and down spins.

For phosphorus, E^{xy} vanishes and we thus expect $\mathbf{H}_{\text{int}}^{\text{P}}$ to lie in the xz plane at an angle with the x axis

$$\theta=\tan^{-1}(E^{xz}/E^{xx}).$$

Figure 10 shows the possible directions for $\mathbf{H}_{\text{int}}^{\text{P}}$ in arrangements (1), (2), and (4). Arrangement (3) should give resonances corresponding roughly to those expected for both arrangements (1) and (2). The resonances would be broadened and shifted because only the two Mn planes nearest to a given phosphorus would correspond to arrangement (1) or (2) and there would be a number of possible arrangements of those Mn planes beyond the closest two but still close enough to affect significantly the field at the phosphorus site. The fact that there is observed in the antiferromagnetic state only one set of relatively narrow phosphorus resonances corresponding to arrangement (1) is taken as strong evidence that (1) is the true arrangement.

Each Li site is a crystallographic center of inversion. In arrangements (1) and (4) Mn inversion pairs have opposite spins. It is easy to show that this condition results in complete cancellation of fields at Li arising from hyperfine interaction and magnetic dipoles and hence leads to the observed $H_{\text{int}}^{\text{Li}}=0$. As has been discussed above, it is very difficult to predict the magnitude of $H_{\text{int}}^{\text{P}}$. However, we can make a good approximation to $H_{\text{int}}^{\text{Li}}$ for arrangement (2) by assuming no hyperfine interaction and all the magnetism concentrated on the Mn atoms. This leads to $H_{\text{int}}^{\text{Li}}$

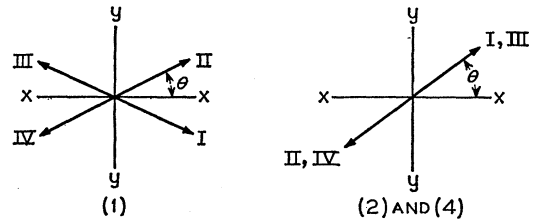

FIG. 10. Directions of $\mathbf{H}_{\text{int}}^{\text{P}}$ for different possible antiferromagnetic spin arrangements numbered as in text. The angle θ would in general be different for different arrangements.

$=6074$ G. There would be four directions as in (1) of Fig. 5 with the difference that in this case the vectors would close to the xy plane, each being lifted out of this plane in the same direction by 1.5°. The angle with the x axis would be 56°. Thus, the observed single narrow resonance of Li corresponding very closely to $H_{\text{int}}^{\text{Li}}=0$ again rules out arrangements (2) and (3) and fortifies the conclusion reached from the phosphorus resonances that (1) is the true arrangement.

It is interesting to note that, although this was not the way it was actually done, the magnetic structure could be worked out on the basis of the paramagnetic and antiferromagnetic nuclear resonance data plus susceptibility data in the paramagnetic state alone, the latter being used only to convince ourselves that the resonances are following the Shulman-Jaccarino picture.

Discussion

It has been seen that the observed antiferromagnetic arrangement of spins in the puckered planes of Mn is just that expected from the network of conventional Mn–O superexchange linkages in these planes. We discuss now the observed correlation between these planes. As has been pointed out above the planes are separated by PO_4 tetrahedra sharing corners and edges with LiO_6 octahedra. The fact that no MnO_6 octahedron from one plane shares any oxygen atom with such an octahedron from another plane means there are no conventional Mn–O–Mn superexchange linkages connecting the planes. The dipolar field at each Mn in the antiferromagnetic state for completely lined up spins is (assuming all magnetism concentrated on Mn) 1276 G for arrangement (2) and 1911 G for arrangement (1), the direction of spin and magnetic field being parallel at each site. This slight energetic advantage for the observed arrangement (1) corresponds to only 0.2°K and hence cannot be an important factor in determining the correlation of planes.

In Sec. 3 it has been established that unpaired s electrons are present on the phosphorus sites and that p electrons may be present. Anderson's picture[4] of superexchange between Mn^{++} ions as antiferromagnetic and as arising from interaction of unpaired electrons carried through covalent bonds suggests that such superexchange could be operative through Mn–O–P–O–Mn linkages. Figure 11 shows Mn atoms in three

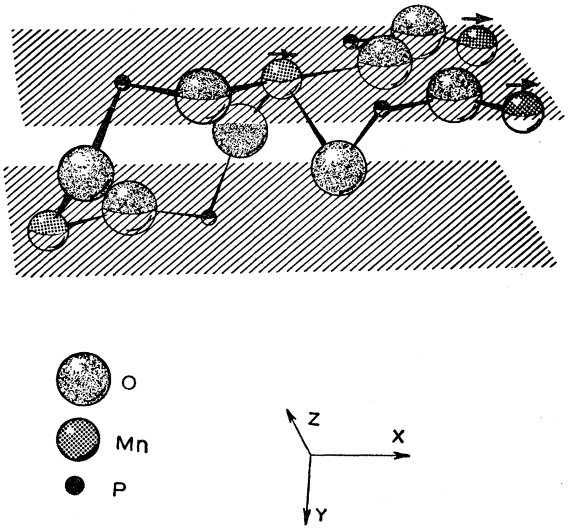

FIG. 11. Mn–O–P–O–Mn linkages between Mn ions in three different puckered planes (left-to-right). Arrows show directions and relative sense of electron spins in the antiferromagnetic state.

planes from left to right. Spin directions are those experimentally observed. Typical Mn–O–P–O–Mn interlinkages in which each Mn is involved are illustrated in this drawing for the central Mn. It is seen that the antiferromagnetic pair is connected by two such linkages. Each Mn is connected to four other antiferromagnetic Mn by such double linkages. Each ferromagnetic pair is connected by only one Mn–O–P–O–Mn linkage and half of these linkages involve the 95° Mn–O–P path which the NMR evidence above indicates is a poor transmitter of magnetism. Each Mn is connected to four other ferromagnetic Mn by such single linkages, two involving 95° Mn–O–P paths. Thus, there are eight antiferromagnetic linkages opposed by two strong and two weaker ferromagnetic linkages for a net of at least four antiferromagnetic. (The Mn–O–Li–O–Mn linkages are such that antiferromagnetic balance ferromagnetic but not necessarily exactly. It has been shown in Sec. 3 that the amount of unpaired s electrons on Li is at most a quarter of that on phosphorus. Therefore, the superexchange effect would be expected to be less and any small unbalance of antiferromagnetic and ferromagnetic linkages should not be important.) Thus, the observed correlation of planes is just that which would be predicted by applying Anderson's picture to Mn–O–P–O–Mn linkages rather than to the usual shorter linkages, e.g., Mn–O–Mn in $LiMnPO_4$. Moreover, the association of nondirect-dipolar NMR shifts intervening anions with superexchange suggested by Shulman and Jaccarino,[2] is further strengthened.

Each Mn is connected to four other antiferromagnetic Mn atoms in the puckered plane by Mn–O–Mn linkages. It has been seen that each Mn has a net of at least four antiferromangetic Mn–O–P–O–Mn linkages to Mn atoms in adjoining planes. It seemed possible that the longer linkages would be sufficiently weaker than the Mn–O–Mn linkages so that there might be observed two Néel temperatures, the higher corresponding to the planes' becoming antiferromagnetic with no correlation between planes and the lower to the planes' becoming correlated. Marshall[26] has interpreted the broad transition observed in $CuCl_2 \cdot 2H_2O$ by susceptibility measurements to the presence of two types of superexchange interaction. In the present case there seems no reason to expect that susceptibility measurements would show any discontinuity except at the initial lining up of spins in the planes. The NMR of both Li and phosphorus should on the other hand show clearly the difference between the two states which of course correspond to arrangements (1) and (3) above. The Li resonance is particularly suitable for investigating this possibility because for arrangement (1) its frequency is not a function of sublattice magnetization and, hence, not a function of temperature. As the temperature rises, there should be a broadening and weakening of the Li NMR at the point where the planes lose their correlation. The observed facts as described in Sec. 3 are that the Li NMR is narrow and shows no discontinuity between 20 and 34.85°K where it becomes somewhat stronger and that there is no further discontinuity above 34.85°K. It is concluded, therefore, that there is a single Néel temperature 34.85°K at which the transition is from paramagnetism to three-dimensional antiferromagnetism. From this it seems that the strength of the superexchange along Mn–O–P–O–Mn interlinkages cannot be as much as an order of magnitude less than that along the Mn–O–Mn interlinkages.

7. LINEWIDTHS AND SHAPES

Data on linewidths and shapes are collected in Table V. The widths and shapes of the resolved quadrupole components of the Li^7 NMR are unchanged in going from the paramagnetic to the antiferromagnetic state. The line shape is Gaussian, and the width of ~ 2.7 G is to be compared with 2.3 G derived from the calculated second moment assuming a Gaussian line. In the paramagnetic state the contribution to $1/T_2$ and, hence, to the linewidth calculated on the exchange narrowing basis can be obtained from the equation[2,27]

$$\frac{1}{T_2}=\left(\frac{\pi}{2}\right)^{1/2}\frac{S(S+1)}{3\hbar^2\omega_e}\sum_{i=x,y,z}(\cos^2\theta_i+\tfrac{1}{2}\sin^2\theta_i)E_i^2, \quad (12)$$

where S is the electronic spin and ω_e the exchange frequency. The sum is over the three principal axes of the $\mathbf{E}=\kappa A+D$ tensor and θ_i is the angle between the ith principal axis and $\mathbf{H}_0$. Estimating ω_e from the

[26] W. Marshall, J. Phys. Chem. Solids, **7**, 159 (1958).
[27] T. Moriya, Progr. Theoret. Phys. (Kyoto) **16**, 23, 641 (1956).

Table V. Experimentally determined linewidths (δH), shapes, and spin-lattice relaxation times (T_1) of Li^7 and P^{31} nuclear resonances in $LiMnPO_4$.

	Antiferromagnetic 4.2°K	Antiferromagnetic 20.3°K	Paramagnetic 77.3°K	Paramagnetic 300°K
		Li		
δH_{obs} (G)	2.7	2.7	2.7	~2.5
Shape	Gaussian	Gaussian	Gaussian	
T_1 (sec)	0.2	0.004	~0.004	
		P		
δH_{obs} (G)	30		2.2	
Shape			Gaussian	

expression

$$\omega_e=\frac{k\theta_N}{\hbar}\left(\frac{6}{ZS(S+1)}\right)^{1/2}. \tag{13}$$

For $\theta_N=77°K$, calculated using $\chi=C/(T+\theta_N)$ and $\chi^{77°K}$ and $\chi^{295°K}$ from Appendix A, and Z the number of superexchange neighbors, taken as 6, we get $\omega_e\sim1.55\times10^{12}$. This gives $1/T_2=0.40\times10^3$ sec^{-1}. and for the Lorentzian shape expected for this mechanism $\delta H=2/\sqrt{3}\gamma T_2\sim0.05$ G which is small compared with the nuclear dipole contribution calculated above from the second moment. Thus the experimental results for the Li^7 resonance are consistent with the theory.

The P^{31} NMR has a Gaussian shape at 77°K and a width of ~2.2 G. The calculated nuclear dipolar second moment gives $\delta H=1.6$ G for a Gaussian line. If we assume that second moments derived from different sources add to give the second moment of the resonance the contribution from exchange narrowing is 1.4 G. This is to be compared with 2.2 G calculated from Eq. (12).

The phosphorus resonance in the antiferromagnetic state is easily seen only under dispersion conditions and even then is distorted, presumably by saturation. Thus, the shape is neither Gaussian nor Lorentzian. Suhl[28] has derived the following expression for the rms linewidth of nuclear resonances of atoms with appreciable hyperfine interaction.

$$(\langle\Delta\nu^2\rangle)^{1/2}=S\left[\frac{I(I+1)}{24\pi}\right]^{1/2}\left(\frac{H_{ex}}{H_{int}}\right)^{1/4}\left(\frac{A}{h}\right)\left(\frac{A}{g\mu_B H_{ex}}\right). \tag{14}$$

The nuclear spin I is that of the magnetic ion and H_{ex} is the exchange field. The expression above refers to the NMR of the magnetic ion itself and A is the hyperfine interaction constant of the magnetic ion. In the present case (NMR of nonmagnetic ion) A^2 is replaced by $A_{Mn}A_P$.[29] Using the values[28] $A_{Mn}=0.01$ cm^{-1} and $A_P\approx A_P{}^s=4.34\times10^{-14}$ cm^{-1} and taking $g\mu_B H_{ex}=\hbar\omega_e$ we obtain an rms linewidth of 28 kc/sec corresponding to $\delta H=56$ kc/sec for a Gaussian shape. This is quite satisfactory agreement with the observed 30 kc/sec, considering the approximations involved.

[28] H. Suhl, Phys. Rev. **109**, 606 (1958).
[29] H. Suhl (private communication).

8. SPIN-LATTICE RELAXATION TIMES

The size of the single-crystal samples available made the NMR signal-to-noise ratio poor enough at low rf so that determination of T_1 was difficult for Li and all but impossible for phosphorus. The values obtained for Li and shown in Table V, were obtained by the saturation method. The rf field H_1 was calibrated from a saturation measurement on NH_4Cl for which T_1 was taken as 0.01 sec.[30] We can calculate T_1 in the paramagnetic state from the expression[2,27]

$$\left(\frac{1}{T_1}\right)=\left(\frac{\pi}{2}\right)^{1/2}\frac{S(S+1)}{3\hbar^2\omega_e}\sum_{i=x,y,z}\sin^2\theta_i E_i{}^2. \tag{15}$$

Using the same data as in computing linewidths above one obtains a value $\sim2\times10^{-3}$ sec for T_1 of Li^7 at 77°K. This is to be compared with the rough experimental value of $\sim4\times10^{-3}$ sec, giving a better agreement than might be expected. The values of T_1 for Li in the antiferromagnetic state have roughly the dependence on T/T_N calculated by Moriya[27] for the proton resonance in $CuCl_2\cdot2H_2O$ (i.e., a resonance relatively unaffected by hyperfine interaction) with the actual values an order of magnitude shorter. It is felt that the number of parameters that must be estimated makes it unprofitable to attempt to fit the data more closely.

9. SUMMARY

(1) The presence of 0.4% of an unpaired 3*s* electron on the phosphorus atom in paramagnetic $LiMnPO_4$ has been established. The phosphorus atom is a second-nearest neighbor to the magnetic Mn^{2+} ions, being separated from it by an oxygen of the $PO_4{}^{3-}$ group. (2). The *transmission* of unpaired electrons to the second-nearest neighbor is found to be consistent with the usual criteria for *superexchange* between second-nearest neighbors as regards σ paths but not as regards π paths. (3). The antiferromagnetic structure of $LiMnPO_4$ has been established by a combination of NMR and susceptibility data. (4). The antiferromagnetic structure determined requires the presence of superexchange interactions along Mn–O–P–O–Mn paths, thus adding to the evidence for the connection between NMR shifts and superexchange. The magnetic structure is just that which would be predicted by application of Anderson's theory of superexchange to Mn–O–P–O–Mn linkages.

ACKNOWLEDGMENTS

The author wishes to thank J. L. Durand for his help in all parts of the experimental investigation, Dr. J. W. Nielsen for growing the single crystals used, Dr. S. Geller for his refinement of the structure of $LiMnPO_4$ and for much advice in crystallographic matters, Dr.

[30] E. M. Purcell, Physica **17**, 282 (1951).

R. M. Bozorth and Dr. S. Foner for susceptibility measurements, Miss B. Cetlin for help in computations, and Dr. P. W. Anderson, Dr. A. M. Clogston, Dr. R. G. Shulman, Dr. H. Suhl, and Dr. L. R. Walker for helpful discussions.

APPENDIX A

Values of magnetic susceptibilities of $LiMnPO_4$ in the paramagnetic state used in this work are as follows:

$$\chi_m^{295°K}=0.01283 \text{ cm}^3 \text{ mole}^{-1}$$
$$\chi_m^{77°K}=0.0310 \text{ cm}^3 \text{ mole}^{-1}. \quad \text{(A1)}$$

The value at liquid-nitrogen temperature was determined by the author, using a single crystal of arbitrary orientation, with a vibrating coil magnetometer.[31] Dr. Simon Foner[32] very kindly made a check of this value with a single-crystal sample provided by the author and obtained a value 0.0312 cm^3 $mole^{-1}$. He also measured the $\chi_m^{295°K}$ given above and for rotation in an arbitrarily chosen plane found the anisotropy was less than one-half percent at both temperatures.

Susceptibility measurements made by Bozorth and Kramer on a mineral crystal $Li(Mn_{0.7}Fe_{0.3})PO_4$ have been published elsewhere.[8] In addition Dr. Bozorth[18] was kind enough to measure the susceptibility of pure $LiMnPO_4$ from 1.4 to 77°K with $\mathbf{H}_0 \| y$ and $\mathbf{H}_0 \| x$.

The time-average magnetic moment of the Mn ion $\langle\mu\rangle$ is needed to go from the geometrical dipole sum tensor elements (A^{-3}) to NMR shifts in gauss or kc/sec. All the measurements in the paramagnetic state were made at $H_0 \approx 9013.5$ G and so $\langle\mu\rangle = \chi_m H/N = 464$ G A^3 at 77°K. For P^{31} this is 800 kc/sec and Li^7 768 kc/sec. The Bohr magneton is 9273.1 G A^3 and so $\langle\mu\rangle$ is 0.0500 Bohr magnetons or 1% lined up in the experiments at liquid-nitrogen temperature. In the antiferromagnetic state at 4.2°K the spins are almost completely lined up and hence $\langle\mu\rangle = 5$ Bohr magnetons and the factors become 4.64×10^4 G and 8.00×10^4 kc/sec for P^{31} and 7.68×10^4 kc/sec for Li^7.

APPENDIX B

In this Appendix we show the conditions under which an NMR at some site in an antiferromagnet can be seen (assuming proper relaxation time and sufficient nuclear moment) with a spectrometer-magnet system of maximum frequency ν_{max} and maximum external field $H_{0(max)}$. We choose two methods of searching. One is to sweep frequency at "zero" external field. In induction instruments if there are two degenerate resonances corresponding to equal but oppositely directed internal fields the signals produced are equal but opposite in phase and hence yield no net signal. This is remedied by applying an external field, of the order of the linewidth, which splits the degeneracy.

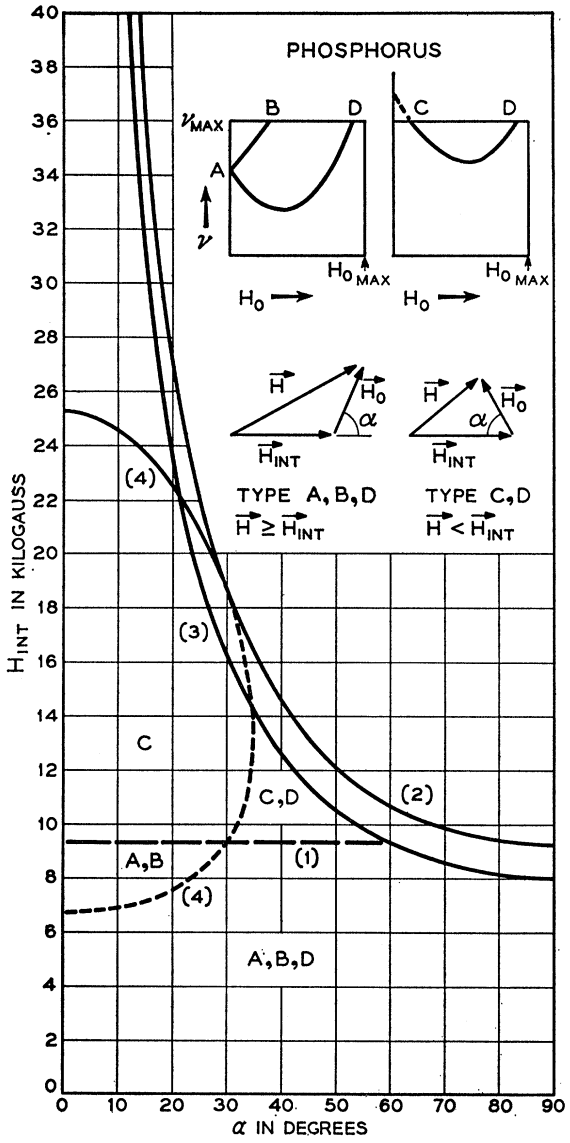

FIG. 12. Detectability of P^{31} nuclear resonances in antiferromagnetic crystals. Regions are marked to show types of resonances (indicated in inset) visible when conditions correspond to a point in the region. See Appendix B.

Resonances seen in this type of search will be called type A (see insert of Fig. 12). In the second type of search the frequency is fixed at ν_{max} and H_0 is swept from near zero to $H_{0(max)}$. The three ways in which resonances can be seen under these circumstances will be called types B, C, and D (Fig. 12).

Before describing the significance of the boundary curves in Fig. 12, we discuss conditions near the minima in the H versus ν curves with $\alpha > 90°$ in Fig. 6. At this minimum, which occurs at $H_0/H_{int} = -\cos\alpha$, the resultant $\mathbf{H}$ is perpendicular to $\mathbf{H}_0$. NMR probes are arranged so that the modulation field is parallel to $\mathbf{H}_0$ and the axis of the rf transmitter coil is perpendicular

[31] S. Foner, Rev. Sci. Instr. **30**, 548 (1959).
[32] S. Foner (private communication).

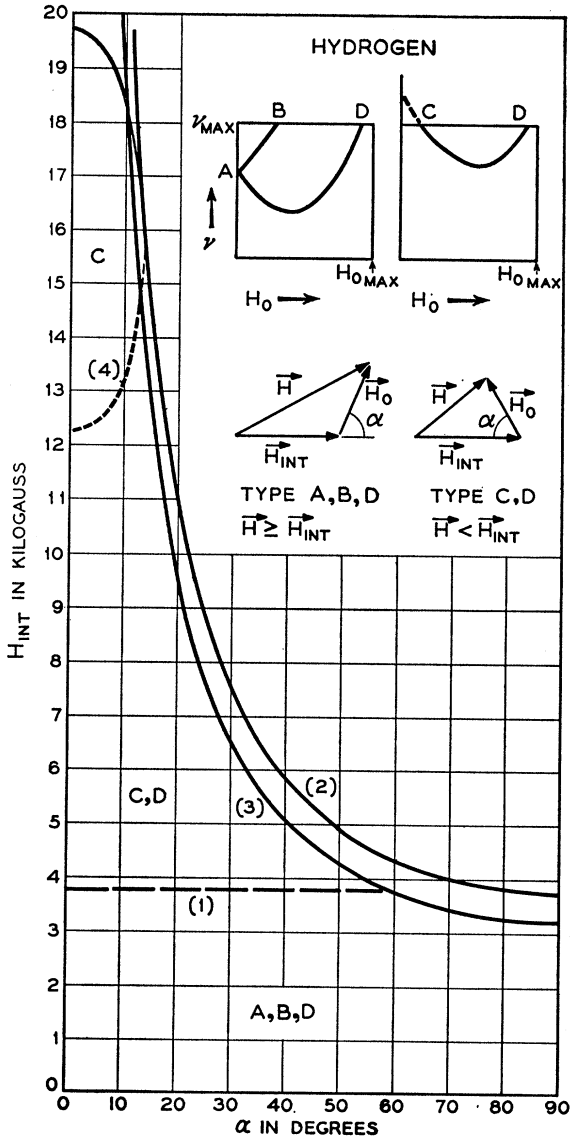

FIG. 13. Detectability of proton nuclear resonances in antiferromagnetic crystals. Compare Fig. 12 and Appendix B. Note ordinate scale is different from Fig. 12.

to $\mathbf{H}_0$ ($\equiv\mathbf{H}$ normally). In the present case $\mathbf{H}$ is perpendicular to $\mathbf{H}_0$, and the modulation is thus ineffective ($dH/dH_0=0$) and the coupling to the rf field will also be zero if $\mathbf{H}$ coincides with the direction of the rf transmitter coil. Thus, the signal is always zero at the minimum if field modulation is used and may be zero even for frequency modulation if the direction of $\mathbf{H}_{\text{int}}$ is such that $\mathbf{H}$ is parallel to the transmitter coil axis. (In case of single coil apparatus substitute the coil axis for transmitter coil axis in the above argument.) Thus, with field modulation the signal always becomes weaker as one approaches the minimum and disappears altogether at the minimum. For $\alpha=180°$ the minimum comes when $\mathbf{H}_0$ exactly cancels $\mathbf{H}_{\text{int}}$, which condition corresponds to zero field at the nucleus; for higher values of H_0 the net field then is opposite in direction to $\mathbf{H}_{\text{int}}$. The four boundary curves drawn in Fig. 12 are as follows:

$$H_{\text{int}}=2\pi\nu_{\max}/\gamma. \tag{B1}$$

This is the absolute upper limit of H_{int} allowing observation of a type A resonance.

$$H_{\text{int}}=(2\pi\nu_{\max}/\gamma)\csc\alpha. \tag{B2}$$

For a given α this expression gives the H_{int} at which type C and D intersections become the same, i.e., where the minimum of the ν versus H_0 curve is at $\nu=\nu_{\max}$. Curve (2) thus gives the absolute maximum H_{int} for which type C and D resonances are observable.

$$H_{\text{int}}=(2\pi\nu_{\max}/1.155\gamma)\csc\alpha. \tag{B3}$$

As has been pointed out above, the resonance at the minimum of the ν versus H_0 is not always observable. This expression gives the H_{int} for which β, the angle between $\mathbf{H}$ and $\mathbf{H}_0$, is 60° for type C and D resonances. This value of β was chosen arbitrarily as given a practical maximum H_{int} for observing these resonances. It is to be noted that with this condition, for $\alpha>60°$, some resonances with $H_{\text{int}}<2\pi\nu/\gamma$ cannot be seen.

$$H_{\text{int}}=\frac{H_{0(\max)}{}^2-(2\pi\nu_{\max}/\gamma)^2}{H_{0(\max)}\cos\alpha\pm[H_{0(\max)}{}^2\cos^2\alpha-H_{0(\max)}{}^2+(2\pi\nu_{\max}/\gamma)^2]^{1/2}}. \tag{B4}$$

This curve is tangent to curve (2). The upper part of the curve, from the point of tangency to the vertical axis gives the maximum H_{int} for which at angle α, a type C resonance occurs (at $H_0\leq H_{0(\max)}$). It is, therefore, an absolute maximum of detectability taking precedence over curves (2) and (3) at angles up to the abscissa of the point of tangency. The lower part of the curve gives the maximum H_{int} for which, at angle α, a type D resonance occurs [at $H_0\leq H_{0(\max)}$]. The point of tangency of curves (2) and (4) corresponds to the conditions where the minimum of the H versus ν curves is at the point $[H_{0(\max)}, \nu_{\max}]$.

In Figs. 12 and 13 the curves are drawn for P^{31} and H^1, the latter to illustrate how curve (4) changes position for a different nucleus. The curves are drawn for $\nu_{\max}=16$ Mc/sec and $H_{0(\max)}=16$ kG.